Desalination and Water Treatment
www.deswater.com
doi:10.5004/dwt.2020.25262

183 (2020) 121–130
April

Fabrication of nanocomposite forward osmosis hollow fiber membrane for low reverse salt flux by modification of active layer via co-extrusion with graphene oxide

Kyunghoon Jang[a,§], Joohwan Lim[a,b,§], Jangho Lee[a], Abayomi Babatunde Alayande[a], Bumsuk Jung[b,*], In S. Kim[a,*]

[a]*Global Desalination Research Center (GDRC), School of Earth Sciences and Environmental Engineering, Gwangju Institute of Science and Technology (GIST), 123 Cheomdangwagi-ro, Buk-gu, Gwangju 61005, Korea, Tel. +82 62 715 2436; Fax: +82 62 715 2584; email: iskim@gist.ac.kr*
[b]*Laboratory of Environmental and Energy Materials, Department of Environmental Engineering and Energy, Myongji University, Yongin, Gyeonggi-do 449-728, Korea, Tel. +82 31 322 6694; Fax: +82 31 336 6336; email: bjung@mju.ac.kr*

Received 23 August 2019; Accepted 27 November 2019

ABSTRACT

One of the rising technology forward osmosis (FO) process enables to reduce the cost of seawater desalination. As such as reverse osmosis process, water transfers through the semi-permeable membranes which are rejected to salts. However, the driving force of FO is not a hydraulic pressure gradient but an osmotic pressure gradient. To get a successful FO process, the membrane of FO should have high salts rejection features, high water permeability, and stability. Graphene oxide (GO) contained membranes are well known for alternative FO membranes due to its high water permeability property. However, another property of GO in membrane fabrication was verified in our study. It was found in our research that reverse salt flux was significantly reduced to 0.06 mol m^{-2} h^{-1} using 2.0 M NaCl draw solution when GO was applied to the active layer of the membrane. Although there have been occasional reports of the use of GO to improve reverse salt flux performance rather than water flux performance improvement. In our study, however, GO was applied only to the localized active layer, resulting in a remarkably reduced reverse salt flux results. In addition, GO was used for the fabrication of hollow fiber membranes.

Keywords: Graphene oxide; Hollow fiber membrane; Mixed matrix membrane; Polyamide; Thin film nanocomposite

1. Introduction

In recent years, accelerating population growth and activities have caused anthropogenic climate change, affecting the global environment and life [1]. Water stress is increasing especially due to the lack of freshwater [2,3]. Consequently, research and development of seawater desalination technology are constantly in progress to supply the shortage of water resources in reverse osmosis (RO) process. However, the development of the RO process is already saturated to reduce energy consumption. To reduce energy cost, there are various attempts to modify RO process plants. Recently, among these miscellaneous trials, forward osmosis (FO) process is in the spotlight for reducing energy cost [4].

The FO process which is powered osmosis pressure gradient as a driving force uses a concentration polarization phenomenon that occurs when a film composed of thin-film composite (TFC) is provided between liquids of

* Corresponding author.

§ The authors are co-first authors. They contributed this research equally.

Presented at the 12th International Desalination Workshop (IDW2019), 28–30 August 2019, Jeju, Korea

different concentrations [5]. Compared to RO, which is powered hydraulic pressure gradient as a driving force and driven by high operating pressures of 50–60 bar, energy can be dramatically reduced, and many studies have been conducted for several years [6].

However, the FO process is difficult to use as a single process, and there are few cases of commercialization due to low water permeability. For these reasons, research steered towards improving water permeability is being actively conducted. Many mixed matrix membranes contain hydrophilic nanomaterials to improve water permeability of separation membranes, and various nanomaterials such as carbon nanotube, graphene oxide (GO), metal-organic framework, and zeolite have attracted interest [7–10].

Among them, GO has been studied a lot recently for reasons such as improvement of mechanical strength of the separation membrane and suppression of antifouling [8,11–16] as well as replacement with various effectors.

In general, a TFC separator is synthesized using m-phenylenediamine (MPD) and 1,3,5-benzenetricarbonyl trichloride (TMC) through interfacial polarization. In the case of MPD, it reacts with –OH and –COOH functional groups of GO [16], and acts as an amide linking ring for interfacial polymerization. If GO is added to the interfacial polymerization, the polyamide (PA) layer thickness, water flux and reverse salt flux will be affected. The more GO added, the higher the crosslinking ratio of the generated PA, which makes it possible to obtain a thin and dense PA layer. When the reverse salt flux is lowered in the FO process, the fouling of the separation membrane is reduced, which can be an advantage in the durability and maintenance of the separation membrane.

In this research, the properties of GO and MPD was used to produce a separation membrane with improved low salt flux in the FO process, likewise, the performance of the separation membrane was evaluated.

2. Experimental section

2.1. GO preparation and characterization

GO was prepared by a modified Hummers method proposed by Jang et al. [17] GO was chemically exfoliated from natural graphite (~325 mesh, Alfa Aesar) via modified Hummers method. 95% of sulfuric acid (H_2SO_4, OCI Co. Ltd.) was prepared in a glass beaker to be mixed with potassium persulfate ($K_2S_2O_8$, OCI Co. Ltd.) and phosphorus pentoxide (P_2O_5, Daejung Chemicals & Materials Co. Ltd.). And then, natural graphite was added to the mixture and boiled to 80°C for half the day with continuous stirring. The mixture was naturally cooled down and vacuum-filtered by a nylon filtration membrane and dried off at room temperature. The resulting substance is called pre-oxidized graphite. Dispersed pre-oxidized graphite solution in 95% of H_2SO_4 was placed in an ice bath. After fully dispersed, potassium permanganate ($KMnO_4$, OCI Co. Ltd.) was spooned slowly into the mixture, and boil to 35°C for half the day with stirring. The oxidized graphene solution was mixed with deionized water, and the next hydrogen peroxide (H_2O_2, OCI Co. Ltd.) droplet was added to the solution until the color changed to yellow. The resulting solution was quenched with 10% hydrochloric acid (HCl, OCI Co. Ltd.) and then rinsed by deionized water. The dialysis process against deionized water was applied for purifying rinsed GO solution using the dialysis tubing membrane (molecular weight cut off of 6–8 kDa, Spectrum Laboratories, Inc.). The finished product GO was obtained after drying the process at 50°C. The characterization of GO was investigated by Fourier transform infrared spectroscopy (FT-IR, iS20 FT-IR spectrometer, Thermo Scientific™ Nicolet™).

2.2. Hollow fiber fabrication process

2.2.1. Dope solution preparation

Well dissolved polyethersulfone (PES, BASF Corp.) dope solution was prepared by simple stirring of mixed polymer solution in the ratio of PES: polyethylene glycol (PEG, Samchun Pure Chemical Co. Ltd.): N,N-Dimethylacetamide (DMAC, Samchun Pure Chemical Co. Ltd.) = 20:60:20 (wt.%). 400 g of PES was put in the dried glass jar and 1,200 g of PEG was put into the jar to wet the contained PES. And then, 400 g of DMAC was mixed with the mixture. The whole mixture was stirred at 180 R.P.M. for 18 h below room temperature. After dissolving, the color of the solution changed to a transparent brown. To preserve the resulting solution in the original state, it was transported into the container and sealed properly.

2.2.2. GO contained bore solution preparation

Bore solution consisted of three kinds according to the GO concentration. GO concentrations were 0, 0.05, and 0.2 mg mL^{-1} in aqueous solution. According to the GO concentration, the name of each sample was identified as 0 mg mL^{-1} to pristine hollow fiber (HF), 0.05 mg mL^{-1} to GO-HF-1, and 0.2 mg mL^{-1} to GO-HF-2. To prepare a specific concentration of GO solution, 12.5 and 50 mg dried GO sheets were weighed. The GO sheets were dispersed in 250 mL of deionized water by sonication for 12 h. The dispersed GO aqueous solution was mixed with 234 g of DMAC by stirring. After 12 h stirring, the fully dispersed GO contained bore solution was prepared.

2.2.3. HF membrane fabrication condition

The HFs were fabricated by the HF spinning machine as shown in Fig. 1. The condition of the spinning machine operation process was detailed in Table 1. The temperature of the water bath was set to 50°C. The configuration of nozzle construction consists of a 0.4 mm inner diameter for bore solution line, 0.2 mm thickness of gap, and 1.5 mm outer diameter for dope solution line. Dope solution and bore solution was supplied into each container chamber. After set up, dope solution supplement gear pump speed and bore solution supplement gear pump speed were set at each 20 and 15 R.P.M separately. And take-up winder speed was set at 2.5 m min^{-1}.

2.3. Porosity measuring

To measure the porosity of the prepared membranes, the dried membranes were cut to a length of 5 cm, weighed

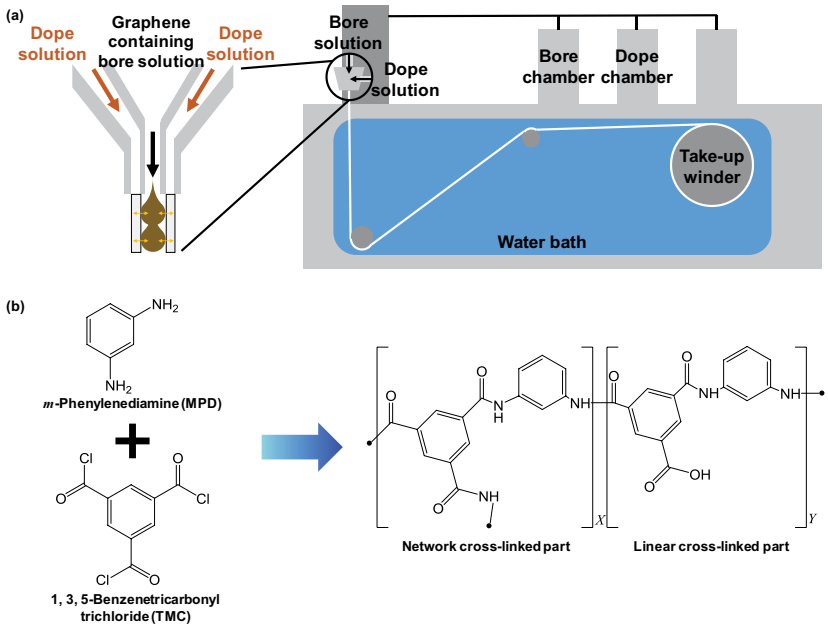

Fig. 1. (a) Schematic diagram of the hollow fiber membrane extrusion process and (b) structural formula of polyamide interfacial polymerization.

Table 1
Hollow fiber extrusion process condition according to the graphene concentration

Sample	D.I. water (mL)	GO (mg)	DMAC (g)	Dope supply gear pump (R.P.M.)	Bore supply gear pump (R.P.M.)	Take-up winder (m min^{-1})
Pristine	–	–	–	20	15	2.5
GO-HF-1	250 mL	12.5 mg	234 g	20	15	2.5
GO-HF-2	250 mL	50.0 mg	234 g	20	15	2.5

Preparation of 0.2 and 0.05 mg mL^{-1} GO mixed bore solution in condition of D.I. water: DMAC = 1:1 (vol.%).

and submerged into isopropanol (OCI Co. Ltd.) for 24 h. Excessive droplets of isopropanol were removed on the surface with filter paper. And the weight of isopropanol contained membranes was measured. Finally, the porosity can be calculated by the below equation.

$$\in = \frac{\left(m_w - m_d\right)/\rho_w}{\frac{m_w - m_d}{\rho_w} + \frac{m_d}{\rho_m}} \quad (1)$$

where m_w is the mass of isopropanol, m_d is the mass of dried membrane, is the density of isopropanol (0.786 g cm^{-3}) and ρ_m is the density of PES (1.37 g cm^{-3}).

2.4. Evaluation of pure water permeability

The pure water permeability (PWP) was measured by deionized water penetrating each support membrane without the PA layer. It was measured from the lumen of HFs to the shell side. Before the measurement, the system was in a steady state at 1.5 bar for 30 min. After the system was maintained at 1.0 bar, the mass of pure water that was passed through the membranes was measured. Finally, the PWP was calculated by Eq. (3).

$$J_w = \frac{V}{\Delta t \times A} \quad (2)$$

$$\text{PWP} = \frac{J_w}{\Delta P} \quad (3)$$

where J_w is the water flux, Δt is the time during the water permeated, A is the area of lumen side and ΔP is the hydraulic pressure difference.

2.5. Interfacial polymerization of PA on the support membrane

2 wt.% of (MPD, Sigma-Aldrich, Inc.) aqueous solution was fed to the lumen side of support membranes for 7 min. The flow rate of MPD was 4.68 mL min^{-1} and excess of MPD droplet was eliminated by purging a sweeping air for 2 min. The 0.15 wt.% of TMC (Tokyo Chemical Industry Co. Ltd.) in n-Hexane (flow rate was 2.78 mL min^{-1}, OCI Co. Ltd.) was brought into contact with the MPD which saturated on the membrane's lumen side, leading to a thin film of PA as a

selective active layer of support membranes. Heat treatment was performed at 70°C oven for 15 min and stored in D.I. water before using.

2.6. GO-HF membrane materials characterization

The lumen side and cross-section morphology confirmation of support membranes, GO-HFs and pristine HFs membranes were conducted by field-emission scanning electron microscopy (FE-SEM, S-4700, Hitachi, Japan). To get tidy cross-section images of membranes, the support membranes, GO-HFs, and pristine HFs membranes were wet by ethanol and frozen by liquid nitrogen. The fully frozen support membranes, GO-HFs and pristine HFs membranes were cut in half and attached on the side of a specimen holder vertically. The cross-linking percentage of pristine HFs and GO-HFs were surveyed by X-ray photoelectron spectroscopy (XPS, MULTILAB 2000, Thermo Scientific) in a range of 0–1,400 eV. The cross-linking percentage was calculated by using the weight percentage of C, N, and O via two below equation.

$$\frac{\mathrm{O}}{\mathrm{N}} = \frac{(3X+4Y)}{(3X+2Y)} \tag{4}$$

$$(\%)\text{cross}-\text{linking}(\mathrm{CL}) = \frac{(X)}{(X+Y)} \times 100 \tag{5}$$

2.7. Cross-flow FO performance test

FO performance test was progressed in active layer facing feed solution (AL-FS) mode through the HF module system. Briefly, the HF module system fabrication of GO-HF and pristine HF membranes were progressed with a 1-inch polyvinyl chloride column (ArtRyx®) and resin (SKA-2702-S, Shin Kwang Chemicals Co. Ltd.) in lab scale. The schematic diagram of the FO performance test process was displayed in Fig. 3. Two gear pumps (Gear Pump Drive, Cole-Parmer Instrument Co. LLC) were used to circulate the feed and draw solution. The draw solution consisted of sodium chloride (NaCl, OCI Co. Ltd.) aqueous solution of 0.5, 1.0, 1.5, and 2.0 M. Deionized water was used for feed solution. During the FO process, the draw solution flowed over the shell side of GO-HF and pristine HF membranes. In the lumen side, deionized water was passed through the active layer. The water flux was detected by the balance connected to the computer system and it was recorded by RS-Key program in real-time. The reverse salt flux was detected by conductivity meter connected to the computer system and it was recorded by RS-Com in real-time. The whole process was managed at 25°C without pressure difference between the membrane.

2.8. Theoretical calculation of water permeability coefficient A, solute permeability coefficient B, and structural parameter S values from FO experiments

After the FO test had been conducted on the fabricated membrane module. The water permeability coefficient (A, LMH bar^{-1}), and the solute permeability coefficient (B, LMH) of the membrane were calculated based on the results from the FO test. The process of obtaining A and B values is as follows.

$$J_w = A\ln\left(\frac{\pi_{D,b}}{\pi_{D,m}}\right) \tag{6}$$

$$J_s = BC_D \times \exp\left(-\frac{J_w}{A}\right) \tag{7}$$

$\pi_{D,b}$, $\pi_{D,m}$ equals to the osmotic pressure of draw bulk solution and draw side of each membrane. C_D refers to the concentration of the draw solution. Finally, J_w and J_s stand for water flux and solute flux, respectively. All tests were conducted in triplicate and the mean value was used [18].

The structural parameter (S, μm) was described in the equation below. (From the following equation, mass transfer coefficient k is inversely proportional to solute resistance kappa (K), $k = \frac{1}{K}$) [19].

$$J_w = A\left\{\frac{\pi_{D,b}\times\exp\left(-\frac{J_w S}{D}\right)-\pi_{F,b}\times\exp\left(\frac{J_w}{k}\right)}{1+\frac{B}{J_w}\left[\exp\left(\frac{J_w}{k}\right)-\exp\left(-\frac{J_w S}{D}\right)\right]}\right\} \tag{8}$$

$$J_s = B\left\{\frac{C_{D,b}\times\exp\left(-\frac{J_w S}{D}\right)-C_{F,b}\times\exp\left(\frac{J_w}{k}\right)}{1+\frac{B}{J_w}\left[\exp\left(\frac{J_w}{k}\right)-\exp\left(-\frac{J_w S}{D}\right)\right]}\right\} \tag{9}$$

where D is the bulk diffusion coefficient of the draw solute, $\pi_{D,b}$ is the bulk osmotic pressure of the draw solution, $\pi_{F,b}$ is the bulk osmotic pressure of the feed solution, $C_{D,b}$ is the concentration of the draw solution, $C_{F,b}$ is the concentration of the draw solution, $\exp\left(-\frac{J_w S}{D}\right)$ is the dilutive internal concentration polarization and $\exp\left(\frac{J_w}{k}\right)$ is the concentrative external concentration polarization.

3. Results and discussion

3.1. Characterization of support membrane

In this paper, the method of selectively loading GO only on the lumen side of the HF used as the active layer is shown in Fig. 1a. The GO was loaded on the lumen side of the membrane by a simultaneous spinning way using GO contained bore solution. This is the way how to load GO on the active layer as a thin layer. This easy and simple spinning method enabled the advantage of GO to retain on the lumen side of HF. The various functional groups of GO were electrically negatively charged [20–23]. Oxygen based functional groups formed hydrogen bonding with PES, the main component of HFs, in the solution state. And after the solvent

was removed, PES and GO were stacked by Van der Waals forces. This interaction between GO and PES allowed GO to be loaded on the lumen side of HFs during the non-solvent induced phase separation process [24]. After spinning, pristine HF and GO-HFs were soaked in glycerol to remain hydrophilic immediately just after spinning. As the concentration of GO in bore solution increased, the degree of GO loading increased and these affected PWP and lumen side FE-SEM results. The PWP results shown in Table 2 tended to increase as the content of GO increased. Each result was indicated as 344 L m^{-2} h^{-1} bar^{-1} for pristine HFs, 1,256 L m^{-2} h^{-1} bar^{-1} for GO-HF-1, and 1,024 L m^{-2} h^{-1} bar^{-1} for GO-HF-2 separately. In these results, the GO-HF-1 membrane had the highest PWP, GO-HF-2 membrane was next, and the worst was pristine HFs membrane. The reason why PWP increased as a result of applying the GO was that the amount of GO loaded was increased as the concentration of GO in bore solution. The increase of loaded GO on the lumen side of HFs as the increase of GO concentration in bore solution was approved in Figs. 2a–c. According to the precedent research, the hydrophilic GO applied membranes had increased water permeability property [25]. The hydrophilicity of GO is attributed to functional groups of GO and the GO which was used in our co-extrusion process examined by FT-IR to confirm the existence of the hydrophilic functional groups in Fig. 2. There was the absorption of infrared radiation between 3,500~1,000 cm^{-1}. The characteristic attributed to GO functional groups were at (a) ~3,391 cm^{-1} (C=O stretching vibration of ketone or carboxyl), (b) ~3,200 cm^{-1} (O–H stretching vibration of carboxyl), (c) ~1,730 cm^{-1} (C=O stretching vibration of carboxyl), (d) ~1,620 cm^{-1} (C=C stretching vibration of sp^2-hybridized C=C), (e) ~1,400 cm^{-1} (O–H deformation of alcohol), (f) ~1,227 cm^{-1} (O=C–O–R stretching vibration of aromatic ether), (g) ~1,056 cm^{-1} (C–OH stretching vibration of alcohol or hydroxyl), and the broadband between 3,050~3,800 cm^{-1} (hydroxyl with C–OH vibrations from COOH and H_2O) [25,26]. From these results, the GO applied to the lumen side of HFs was confirmed that it is containing hydrophilic functional groups such as carboxyl and hydroxyl. It demonstrated that the increase of GO loaded on the lumen side of HFs induced the increase of water permeability. Furthermore, as shown in the FE-SEM images of Fig. 2a, no stain was observed on the surface of the lumen side pristine HFs membrane, which means that GO was not present on the lumen side surface of the pristine HFs. On the contrary, in the case of GO-HF-1, it was confirmed that the GO was smeared overall. In the case of GO-HF-2, which was made of a bore solution with a higher GO content than GO-HF-1, the lumen side was stained by GO as such as GO-HF-1. In addition, the more and thicker GO flakes have been identified on the lumen side surface of GO-HF-2 than GO-HF-1. In other words, it was confirmed that excessive GO was loaded on the surface of the lumen side as the GO content increases in the bore solution, causing the formation of immoderate GO flakes on the surface. On the other hand, in terms of porosity, GO did not affect the structure of the entire HFs. From the average porosity results in Table 2, the results of pristine HFs membranes, GO-HF-1 membranes, and GO-HF-2 membranes have shown almost similar values. These results demonstrated that GO did not directly participate in HFs structural change but only adhered to the surface of the lumen side to be an active layer on the cross-sectional images of Figs. 3–i. No significant structural changes were observed at low magnification. Similarly, it was confirmed that at high magnification, the monolith structure of HFs support membrane was shown regardless of GO content and presence. This ensured that GO was selectively loaded only on the surface of the lumen side of support membrane, without losing the hydrophilicity properties of GO, and the degree of GO loading was able to be controlled by the concentration of GO in the bore solution and did not alter the original structure of support membrane.

Table 2
Pure water permeability (PWP) and porosity of pristine HF and GO-HFs

Sample	PWP (L m^{-2} h^{-1} bar^{-1})	Porosity (%)
Pristine	344	81
GO-HF-1	1,256	82
GO-HF-2	1,024	82

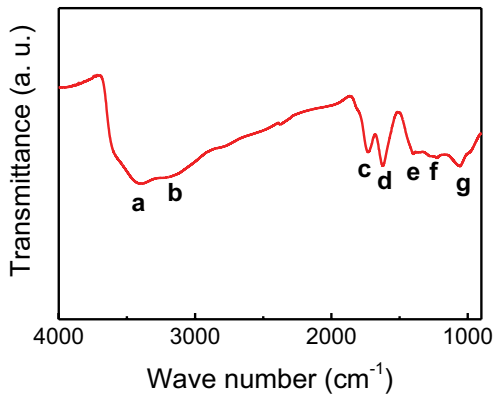

Fig. 2. FT-IR result of GO applied on the lumen side of the HF membrane.

3.2. GO-HF membranes characterization

In general, PA has been used as the active layer of TFC in the desalination process. In this study, PA was applied as an active layer, and PA was formed on the lumen side surface of HFs support membrane through interfacial polymerization of MPD and TMC. In addition, the adsorption between GO and PES which were stacked by Van der Waals force was able to be complemented by the formation of PA on the active layer. In other words, GO was likely to be released by hydrogen bonding with the solution when the aqueous solution flows, but the problem was solved because the PA formed near the functional groups percolated into the structure of the PES. [24,25] Therefore, the pristine HFs membrane, GO-HF-1 membranes, and GO-HF-2 membranes were subject to PA interfacial polymerization after its physical properties evaluation was completed. The functional groups of GO allowed PA to be selectively formed on GO-loaded active layers, and its morphology was confirmed by FE-SEM results on the lumen side surface. Figs. 3b, e, and h are FE-SEM results of pristine HFs membranes, GO-HF-1 membranes, and

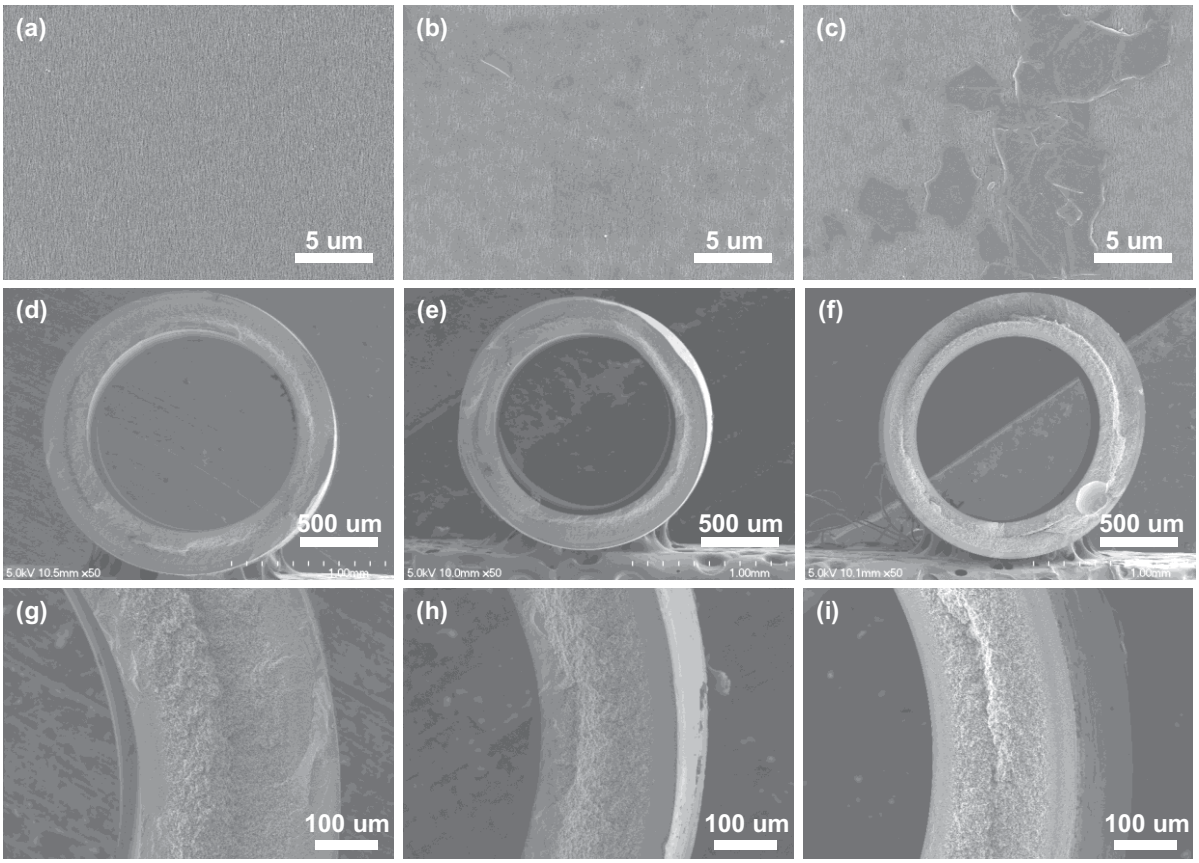

Fig. 3. SEM images of non-PA coated pristine HF and GO-HFs shows on below. The lumen side surface of (a) pristine HF, (b) GO-HF-1, and (c) GO-HF-2 were displayed. The low magnification cross-section image of (d) pristine HF, (e) GO-HF-1, and (f) GO-HF-2 were displayed. And the high magnification cross-section image of (g) pristine HF, (h) GO-HF-1, and (i) GO-HF-2 were displayed.

GO-HF-2 membranes at low-magnifications, respectively. The black stain which is not observed in Fig. 4b, a low-magnification FE-SEM image of pristine HFs membrane, is the part of GO without functional groups in Figs. 4e and h. Since there were parts of the absence of oxygen functional groups on GO flakes, little or no PA was formed near that area, and black spots were observed around the synthesized PA. Those FE-SEM images are shown in Figs. 4e and h of GO-HF-1 membranes and GO-HF-2 membranes separately. As the amount of loaded GO increased, the selectively formed PA area was evenly spread. The high-magnification FE-SEM results are displayed in Figs. 4c, f and i. The uniformly distributed ridge-and-valley structure of PA was confirmed in Fig. 3c the pristine HFs membranes. As shown in Figs. 4f and i separately, the partially distributed ridge-and-valley structure of PA was observed at the edge of GO flakes where the most of oxygen functional groups existed. The cross-section of high magnification FE-SEM images of pristine HFs membranes, GO-HF-1 membranes, and GO-HF-2 membranes is shown in Figs. 4a, d, and g. In cross-section, the well formation of the PA active layer on the lumen side of HFs was confirmed. The PA roughness of GO-HF-2 membranes was less smooth than GO-HF-1 membranes, however, it was smoother than the PA roughness of pristine HFs. The reason why there was a difference in the degree of roughness would be because GO with amphiphilic acted as a surfactant during interfacial polymerization, resulting in a smaller ridge-and-valley structure [25,27,28]. However, the roughness of GO-HF-2 membranes became rougher than GO-HF-1 membranes, because the GO loaded on the surface of the active layer was excessively coated.

The amount of PA formation; the active layer that played the most important role in filtering salt, was determined by calculating the cross-linking percentage of PA chemical structure. The cross-linking percentage of PA was calculated from the atomic weight percentage of carbon, oxygen, and nitrogen determined through XPS measurement which was detected only from the portion of PA on HF membranes, GO-HF-1 membranes, and GO-HF-2 membranes. The calculation method has been described in Eqs. (4) and (5). The results calculated using the atomic weight percentage are summarized in Table 2. The results showed that pristine HFs membranes were the smallest with 55.62%, GO-HF-1 membranes with 60.77%, and GO-HF-2 membranes with the highest cross-linking percentage of 75.47%. The hydroxyl and carboxyl groups in the functional groups of GO electrically attracted the amine groups of MPD, thereby MPD gathered near those functional groups, and resulting in the interfacial polymerization with TMC in the converged MPD region [23,25]. The cross-linking of PA was concentrated in the area where the functional group exists. Hence, the cross-linking was formed in the area of GO flake edge where

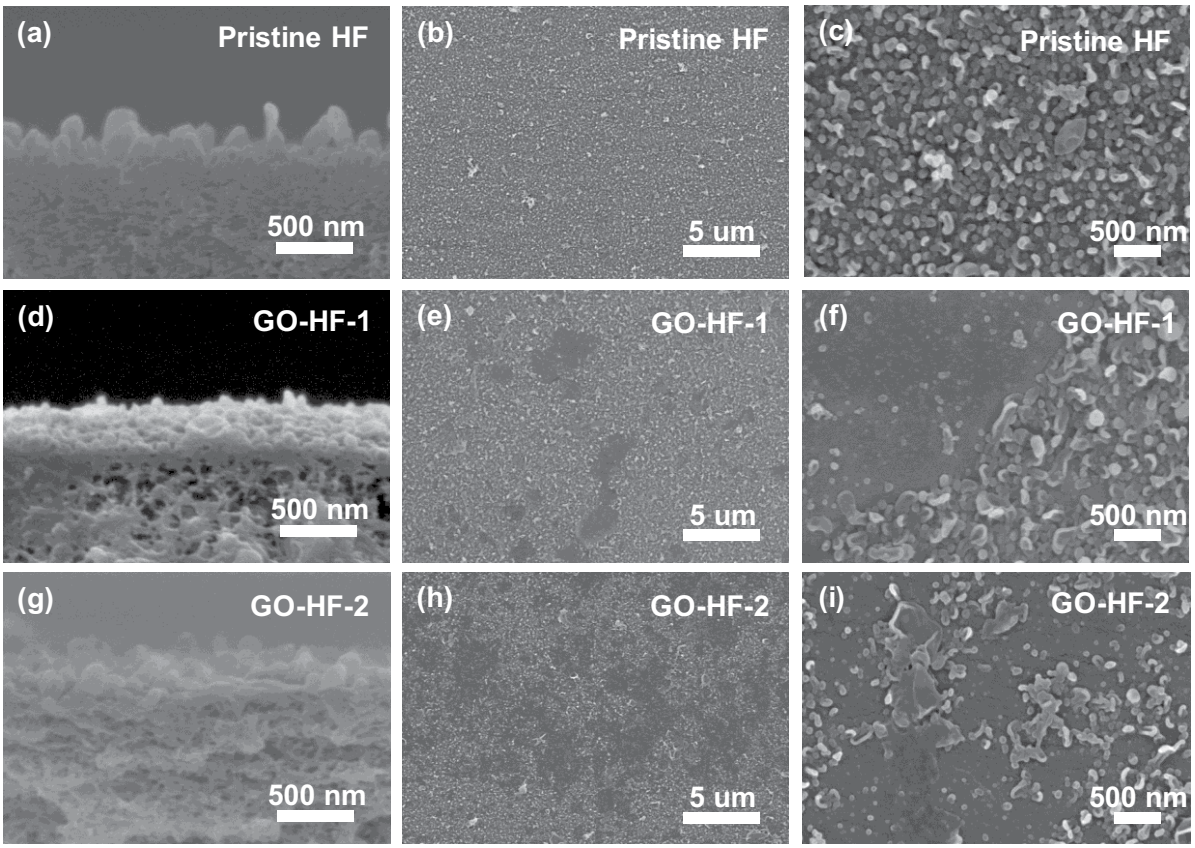

Fig. 4. SEM images of GO-HF membranes. (a) shows cross-section of pristine HF in a high magnification, (b,c) the interior of pristine HF as a low magnification and a high magnification separately, (d) the cross-section of GO-HF-1 in a high magnification, (e,f) the interior of GO-HF-1 as a low magnification and a high magnification separately, (g) the cross-section of GO-HF-2 in a high magnification, (h,i) the interior of GO-HF-2 as a low magnification and a high magnification separately.

the GO functional groups are dominant, and it seems like that the PA channel was formed by the presence of GO functional groups [29]. And the hydrogen bonding contained PA channel can attract water to keep the usual water flux of the TFC membrane [4]. In addition, when the GO concentration of the bore solution increased during the loading of GO, the amount of loaded GO increased, so that the GO functional groups also increased. Consequently, the cross-linking percentage also increased, as the amount of loaded GO increased. These quantitative results are displayed in Figs. 4c, f and i, through the image where the PA was partially formed.

3.3. FO performance

So far, the GO-HFs membranes have been tested for the confirmation of loaded GO and its properties. In this study, GO-HFs membranes were fabricated to be applied for the desalination FO process. Therefore, an FO test using a NaCl solution was performed to evaluate the performance. For the FO test, a 1-inch column module of the laboratory scale was made for applying the manufactured GO-HFs membranes, and the FO test process shown in Fig. 5 was performed. The module production method was discussed in the experimental method. Through the FO test, the results of water flux and reverse salt flux were confirmed, and the results of J_s/J_w, which was about the reverse salt flux per water flux, were also confirmed. Fig. 6 shows the results of the aforementioned experiments with different GO contents. In Fig. 6a the water flux was relatively high in pristine HFs membrane compared to GO-HFs membranes, but the difference was not noticeably large. Compared to the water flux among the three samples at the concentration of 2.0 M NaCl draw solution, the water flux displayed a minimal difference, 15.76 LMH for pristine HF membranes, 14.11 LMH for GO-HF-1 membranes and 14.73 LMH for GO-HF-2 membranes, separately. These results were in contrast to the PWP results mentioned earlier, and the water flux of GO-HF membranes was decreased compared to the water flux of pristine HF membranes. The water flux is influenced by the hydrophilicity of materials, and the hydrophilicity of GO-HF membranes was higher than the pristine HF membrane in previous PWP results due to its hydrophilic functional groups. However, since the oxygen functional groups of GO were bonded with PA after interfacial polymerization, the hydrophilicity of GO-HF membranes was reduced after PA interfacial polymerization process [21,25]. In Fig. 6b the results of reverse salt flux were summarized by GO content and draw solution concentration. Reverse salt flux results in 2.0 M NaCl draw solution showed 0.18 mol m^{-2} h^{-1} for pristine HFs membranes, 0.06 mol m^{-2} h^{-1} for GO-HF-1 membranes, and 0.66 mol m^{-2} h^{-1} for GO-HF-2 membranes.

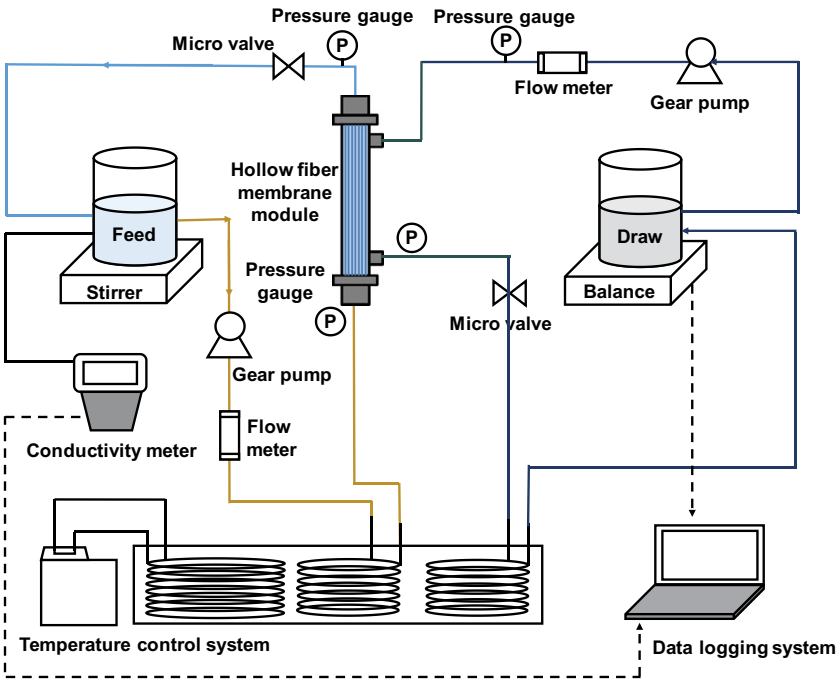

Fig. 5. Schematic diagram of the GO-HF module forward osmosis (FO) test process.

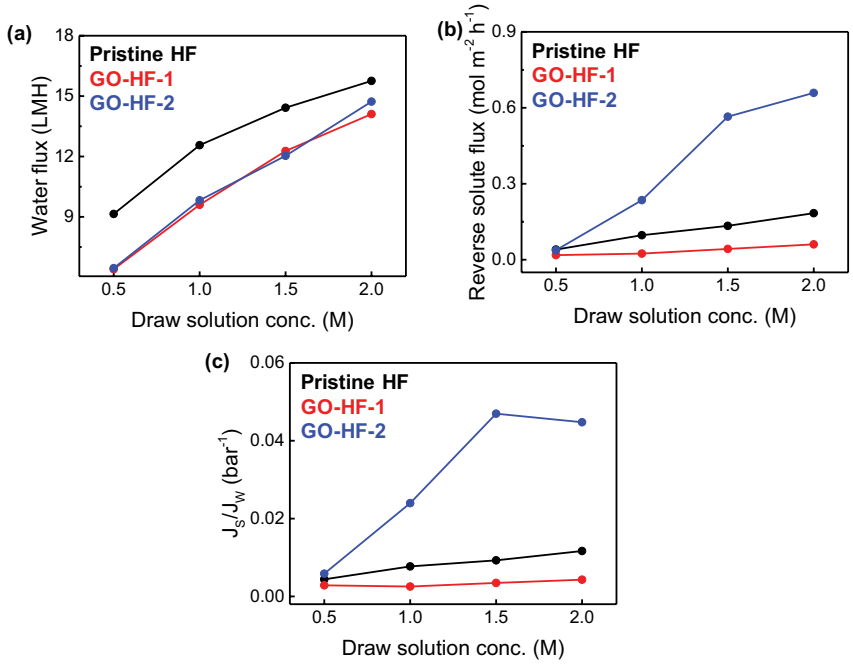

Fig. 6. FO performance of the GO-HF module is shown as (a) water flux, (b) reverse salt flux, and (c) reverse salt flux over water flux ratio (J_s/J_w).

The reverse salt flux of GO-HF-1 membranes was significantly reduced compared to pristine HFs that did not contain GO. Since the graphitic part of GO with less functional groups is hydrophobic, the water flux penetrated the part where the PA acted as a channel. This led to an improvement in reverse salt flux performance. However, in the case of GO-HF-2 membranes, the reverse salt flux was higher than pristine HFs membranes, which was caused by cracking which occurred on GO surface after interfacial polymerization due to excessive GO, namely, some PA-free channels were formed on excessive GO surface, which induced an increase of reverse salt flux. The aforementioned cracks were confirmed by the high magnification lumen side FE-SEM results of Fig. 4i GO-HF-2 membranes. Finally,

Table 3
Cross-linking percentage of polyamide analysis results conducted by X-ray photoemission spectroscopy

Sample	C (At.%)	N (At.%)	O (At.%)	C/N	O/N	CL (%)
Pristine	72.96	11.52	15.52	6.33	1.35	55.62
GO-HF-1	76.60	10.17	13.23	7.53	1.30	60.77
GO-HF-2	77.89	10.16	11.95	7.67	1.18	75.47

Comparison of theoretical value.

a graph comparing the J_s/J_w results is shown in Fig. 6c to confirm the results of the improved reverse salt flux to the water flux. The results in Table 4 show that pristine HFs membranes were 0.012 bar^{-1}, GO-HF-1 membranes were 0.004 bar^{-1}, and GO-HF-2 membranes were 0.045 bar^{-1} in 2.0 M NaCl draw solution. It was similar to the reverse salt flux mentioned. There was no significant change in the water flux compared to that of GO-HFs membranes, but the reverse salt flux performance was greatly improved. Table 4 shows the results of the FO test in 2.0 M NaCl draw solution as *A*, *B*, and *S* values mentioned in experimental part 2.8. In the *A* value of the water flux coefficient, no significant difference was observed among the three samples. However, the difference was significantly observed in the *B* value of the reverse salt flux coefficient and *S* value of the structural parameter. The *B* value of GO-HF-1 membranes was the lowest and showed excellent reverse salt flux results. However, the *S* value was the highest because of the structural parameters *S* value which was described in Eqs. (5) and (6), as shown in 2.8 was affected by *A* and *B* values. In other words, the water flux and reverse salt flux results of the FO test was able to affect the *S* value. Although the water flux of GO-HF-1 membranes was similar to that of other samples, the *S* value calculations were very large compared to other samples because the reverse salt flux was very low compared to other samples. The high *S* value which was only numerical value growth didn't mean that there was an actual structural disadvantage because the salt didn't move well due to the PA channel [16,24]. As noted earlier in Figs. 3d–f, the addition of GO did not result in structural or material differences in support. Therefore, a very high *S* value, which was calculated by using results of *A* and *B* values, showed that the reverse salt flux of GO-HF-1 membranes was significantly improved at similar *A* values. The *A*, *B*, and *S* values results compared with other studies are summarized in Table 4. From Table 4, the *A* values of GO-HF-1 membranes were not much different, but the *B* values of the GO-HF-1 membranes were one-tenth smaller than the results of other studies. This indicated that GO-HF-1 membranes, whose *S* value was 10 times larger than other samples, were the result of excellent reverse salt flux.

Table 4
A, *B*, and *S* values comparison of GO-HF membrane modules and recent research on FO membrane development

Sample	*A* value (LMH bar^{-1})	*B* value (LMH)	*S* value (um)	J_s/J_w (bar^{-1})
Pristine HF	1.055	0.044	265.697	0.012
GO-HF-1	0.860	0.011	1,156.312	0.004
GO-HF-2	1.115	0.172	721.499	0.045
TFC-PES [30]	1.18	0.135	219	0.192
TFC [31]	1.51	0.44	110	0.212

Draw solution 2.0 M of NaCl and feed solution D.I. water, all membrane orientations are AL-FS mode.

4. Conclusion

Until now, other studies have shown that the water flux increases when GO was applied to the membrane. However, in this study, we applied to GO only on the active layer of the HF membrane. Although the water flux was no noticeable change the reverse salt flux was significantly reduced. This could happen by loading the appropriate amount of GO only on the active layer. The oxygen functional groups of GO allowed the selective reaction site of the interfacial polymerization of the PA. In addition, the part of GO in the absence of oxygen functional groups had hydrophobic properties, so the formed PA acted as a channel because the part of GO in the absence of oxygen functional groups blocked the penetration of water. As a result, the TFN membranes, which had no significant change in the water flux but greatly improved reverse salt flux was successfully applied to FO process membranes.

Acknowledgment

This work was supported by the Korea Environment Industry & Technology Institute (KEITI) through the Industrial Facilities & Infrastructure Research Program, funded by the Korea Ministry of Environment (MOE) (1485016274).

References

[1] C. Rosenzweig, D. Karoly, M. Vicarelli, P. Neofotis, Q. Wu, G. Casassa, A. Menzel, T.L. Root, N. Estrella, B. Seguin, P. Tryjanowski, C. Liu, S. Rawlins, A. Imeson, Attributing physical and biological impacts to anthropogenic climate change, Nature, 453 (2008) 353–358.
[2] E. de Nicola, O.S. Aburizaiza, A. Siddique, H. Khwaja, D.O. Carpenter, Climate change and water scarcity: the case of Saudi Arabia, Ann. Global Health, 81 (2015) 342–353.
[3] Y. Wada, L.P.H. van Beek, D. Viviroli, H.H. Dürr, R. Weingartner, M.F.P. Bierken, Global monthly water stress: 2. water demand and severity of water stress, Water Resour. Res., 47 (2011) W07518 1–17.
[4] M. Elimelech, W.A. Phillip, The future of seawater desalination: energy, technology, and the environment, Science, 333 (2011) 712–718.
[5] J.R. McCutcheon, R.L. McGinnis, M. Elimelech, A novel ammonia—carbon dioxide forward (direct) osmosis desalination process, Desalination, 174 (2005) 1–11.
[6] N. Misdan, W.J. Lau, A.F. Ismail, Seawater reverse osmosis (SWRO) desalination by thin-film composite membrane — current development, challenges and future prospects, Desalination, 287 (2012) 228–237.
[7] R. Das, Md. E. Ali, S.B.A. Hamid, S. Ramakrishna, Z.Z. Chowdhury, Carbon nanotube membranes for water purification: a bright future in water desalination, Desalination, 336 (2014) 97–109.
[8] H.M. Hegab, L. Zou, Graphene oxide-assisted membranes: fabrication and potential applications in desalination and water purification, J. Membr. Sci., 484 (2015) 95–106.

[9] E. Elsayed, R. Al-Dadah, S. Mahmoud, P.A. Anderson, A. Elsayed, P.G. Youssef, CPO-27(Ni), aluminium fumarate and MIL-101(Cr) MOF materials for adsorption water desalination, Desalination, 406 (2017) 25–36.
[10] M.L. Lind, A.K. Ghosh, A. Jawor, X. Huang, W. Hou, Y. Yang, E.M.V. Hoek, Influence of zeolite crystal size on zeolite-polyamide thin film nanocomposite membranes, Langmuir, 25 (2009) 10139–10145.
[11] B.M. Ganesh, A.M. Isloor, A.F. Ismail, Enhanced hydrophilicity and salt rejection study of graphene oxide-polysulfone mixed matrix membrane, Desalination, 313 (2013) 199–207.
[12] A. Anand, B. Unnikrishnan, J.-Y. Mao, H.-J. Lin, C.-C. Huang, Graphene-based nanofiltration membranes for improving salt rejection, water flux and antifouling–a review, Desalination, 429 (2018) 119–133.
[13] Z. Xu, J. Zhang, M. Shan, Y. Li, B. Li, J. Niu, B. Zhou, X. Qian, Organosilane-functionalized graphene oxide for enhanced antifouling and mechanical properties of polyvinylidene fluoride ultrafiltration membranes, J. Membr. Sci., 458 (2014) 1–13.
[14] S. Zinadini, A.A. Zinatizadeh, M. Rahimi, V. Vatanpour, H. Zangeneh, Preparation of a novel antifouling mixed matrix PES membrane by embedding graphene oxide nanoplates, J. Membr. Sci., 453 (2014) 292–301.
[15] S.P. Surwade, S.N. Smirnov, I.V. Vlassiouk, R.R. Unocic, G.M. Veith, S. Dai, S.M. Mahurin, Water desalination using nanoporous single-layer graphene, Nat. Nanotechnol., 10 (2015) 459–464.
[16] S. Bano, A. Mahmood, S.-J. Kim, K.-H. Lee, Graphene oxide modified polyamide nanofiltration membrane with improved flux and antifouling properties, J. Mater. Chem. A, 3 (2015) 2065–2071.
[17] K. Jang, D.-K. Hwang, F.M. Auxilia, J. Jang, H. Song, B.-Y. Oh, Y. Kim, J. Nag, J.-W. Park, S. Jeong, S.S. Lee, S. Choi, I.S. Kim, W.B. Kim, J.-M. Myoung, M.-H. Ham, Sub-10-nm Co_3O_4 nanoparticles/graphene composites as high-performance anodes for lithium storage, Chem. Eng. J., 309 (2017) 15–21.
[18] S. Kook, C.D. Swetha, J. Lee, C. Lee, T. Fane, I.S. Kim, Forward osmosis membranes under null-pressure condition: do hydraulic and osmotic pressure have identical nature?, Environ. Sci. Technol., 52 (2018) 3556–3566.
[19] B. Kim, G. Gwak, S. Hong, Review on methodology for determining forward osmosis (FO) membrane characteristics: water permeability (A), solute permeability (B), and structural parameter (S), Desalination, 422 (2017) 5–16.
[20] D. Konios, M.M. Stylianakis, E. Stratakis, E. Kymakis, Dispersion behavior of graphene oxide and reduced graphene oxide, J. Colloid Interface Sci., 430 (2014) 108–112.
[21] S. Park, R.S. Ruoff, Chemical methods for the production of graphenes, Nat. Nanotechnol., 4 (2009) 217–224.
[22] D. Li, M.B. Müller, S. Gilje, R.B. Kaner, G.G. Wallace, Processable aqueous dispersions of graphene nanosheets, Nat. Nanotechnol., 3 (2008) 101–105.
[23] C. Vallés, C. Drummond, H. Saadaoui, C.A. Furtado, M. He, O. Roubeau, L. Ortolani, M. Monthioux, A. Pénicaud, Solutions of negatively charged graphene sheets and ribbons, J. Am. Chem. Soc., 130 (2008) 15802–15804.
[24] F. Li, Y. Liu, C.-B. Qu, H.-M. Xiao, Y. Hua, G.-X. Sui, S.-Y. Fu, Enganced mechanical properties of short carbon fiber reinforced polyethersulfone composites by graphene oxide coating, Polymer, 59 (2015) 155–165.
[25] L. Shen, S. Xiong, Y. Wang, Graphene oxide incorporated thin-film composite membranes for forward osmosis applications, Chem. Eng. Sci., 143 (2016) 194–205.
[26] B.D. Mistry, Handbook of Spectroscopic Data: Chemistry - UV, IR, PMR, CNMR and Mass Spectroscopy, Oxford Book Company, Jaipur, India, 2009.
[27] T. Fujioka, B.E. O'Rourke, K. Michishio, Y. Kobayashi, N. Oshima, H. Kodamatani, T. Shintani, L.D. Nghiem, Transport of small and neutral solutes through reverse osmosis membranes: role of skin layer conformation of the polyamide film, J. Membr. Sci., 554 (2018) 301–308.
[28] M.J. Park, S. Phuntsho, T. He, G.M. Nisola, L.D. Tijing, X.-M. Li, G. Chen, W.-J. Chung, H.K. Shon, Graphene oxide incorporated polysulfone substrate for the fabrication of flat-sheet thin-film composite forward osmosis membranes, J. Membr. Sci., 493 (2015) 496–507.
[29] C.-M. Kim, S. Hong, R. Li, I.S. Kim, P. Wang, Janus graphene oxide-doped, lamellar composite membranes with strong aqueous stability, ACS Sustainable Chem. Eng., 7 (2019) 7252–7259.
[30] P. Sukitpaneenit, T.-S. Chung, High performance thin-film composite forward osmosis hollow fiber membranes with macrovoid-free and highly porous structure for sustainable water production, Environ. Sci. Technol., 46 (2012) 7358–7365.
[31] L. Luo, P. Wang, S. Zhang, G. Han, T.-S. Chung, Novel thin-film composite tri-bore hollow fiber membrane fabrication for forward osmosis, J. Membr. Sci., 461 (2014) 28–38.